Branch specific and spike-order specific action potential invasion in basal, oblique, and apical dendrites of cortical pyramidal neurons

Wen-Liang Zhou
Shaina M. Short
Matthew T. Rich
Katerina D. Oikonomou
Mandakini B. Singh
Enas V. Sterjanaj
Srdjan D. Antic

SPIE.

Branch specific and spike-order specific action potential invasion in basal, oblique, and apical dendrites of cortical pyramidal neurons

Wen-Liang Zhou, Shaina M. Short, Matthew T. Rich, Katerina D. Oikonomou, Mandakini B. Singh, Enas V. Sterjanaj, and Srdjan D. Antic*
University of Connecticut, Stem Cell Institute, Institute for Systems Genomics, UConn Health, Department of Neuroscience, 263 Farmington Avenue, Farmington, Connecticut 06030-3401, United States

Abstract. In neocortical pyramidal neurons, action potentials (APs) propagate from the axon into the dendritic tree to influence distal synapses. Traditionally, AP backpropagation was studied in the thick apical trunk. Here, we used the principles of optical imaging developed by Cohen to investigate AP invasion into thin dendritic branches (basal, oblique, and tuft) of prefrontal cortical L5 pyramidal neurons. Multisite optical recordings from neighboring dendrites revealed a clear dichotomy between two seemingly equal dendritic branches belonging to the same cell ("sister branches"). We documented the variable efficacy of AP invasion in basal and oblique branches by revealing their AP voltage waveforms. Using fast multisite calcium imaging, we found that trains of APs are filtered differently between two apical tuft branches. Although one dendritic branch passes all spikes in an AP train, another branch belonging to the same neuron, same cortical layer, and same path distance from the cell body, experiences only one spike. Our data indicate that the vast differences in dendritic voltage and calcium transients, detected in dendrites of pyramidal neurons, arise from a nonuniform distribution of A-type K^+ conductance, an aggregate number of branch points in the path of the AP propagation and minute differences in dendritic diameter. © *2015 Society of Photo-Optical Instrumentation Engineers (SPIE)* [DOI: 10.1117/1.NPh.2.2.021006]

Keywords: prefrontal cortex; voltage-sensitive dye; voltage imaging; calcium imaging; long term potentiation; dendritic integration.

Paper 14069SSR received Oct. 5, 2014; accepted for publication Nov. 10, 2014; published online Dec. 29, 2014.

1 Introduction

Action potentials (APs) propagate from the axon initial segment into the dendritic tree[1] to depolarize distal dendritic segments, trigger dendritic influx of calcium ions, and influence the integration and long-term efficacy of distal synapses.[2,3] In apical and basal pyramidal dendrites, backpropagating APs decrease in amplitude as they reach progressively distal locations.[1,4] In long (>200 μm) basal dendrites, the attenuation is substantial.[5,6] In short basal dendrites ($\leq$ 150 μm), the AP attenuation slope is not so steep.[7–11] Notable differences in AP backpropagation efficacy exist even among the most homogenous class of dendritic branches, basal dendrites, which are anatomically positioned at the shortest distance from the soma. One must then wonder about the inhomogeneities (in the AP invasion efficacy) that may exist among more distal apical-oblique and apical-tuft branches. Due to the weak excitability of the dendritic membrane[12–14] and the existence of a number of dendritic branch points (BPs) along the path from the soma,[15,16] individual oblique and tuft branches may experience vastly different voltage and calcium transients during the propagation of the same AP. If two sister branches (two basal, two oblique, or two tuft dendrites) experience several-fold different amounts of calcium influx during an AP, then the rules of spike timing-dependent plasticity (STDP)[17–19] will dictate that certain synaptic contacts will be favored in this process merely due to their impinging on one and not another sister branch. This would imply that the formation and function of neuronal circuits depend not only

on synaptic contacts arriving in the precise cortical layer at a precise path distance from the soma, but also on a precise dendritic branch in that layer, as not all sister branches are allowing the same feedback from the axon initiation site, in the form of a backpropagating AP. In the case of axon fibers, notable amplitude heterogeneity was observed in axon varicosities of cerebellar basket cells[20] and cortical pyramidal cells.[21] The first evidence that neighboring regions of the dendritic tree can experience notably different calcium signals during repetitive AP firing came from pioneering studies on hippocampal CA1 pyramidal cells.[16] Here, we used the principles of optical imaging and actual equipment developed by Cohen to investigate the rules of AP invasion in sister branches of layer 5 (L5) pyramidal neurons in the rat medial prefrontal cortex (PFC). Simultaneous optical recordings from neighboring dendrites revealed that the AP-invasion dichotomy is present not only between two cells[22–24] but also between two morphologically similar, seemingly equal branches, belonging to one cell. Specifically, we documented the variable efficacy of AP invasion in basal and oblique branches by revealing AP voltage waveforms. Using calcium imaging, we found that trains of APs are filtered differently between individual apical tuft branches. Although one tuft branch passes all spikes in an AP triplet, another tuft branch belonging to the same neuron, same cortical layer, and same path distance from the cell body, experiences only one spike. By sampling dendritic optical signals with high temporal and spatial resolutions, these data revealed that APs fail at BPs in the apical tuft. Following

the biocytin reconstructions of recorded neurons, we established a negative correlation between AP signal size and dendritic diameter. Thinner branches always experienced larger AP signals than thicker branches in the same dendritic tree. Our modeling study suggests that very large differences in dendritic signal amplitude are most likely due to uneven distribution of dendritic A-type K^+ channels. Further experimentations with A-type K^+ current antagonist (Ba^{2+}) confirmed the ability of such

K^+ conductance to modulate the AP amplitude-ratio between sister branches corroborating our model's predictions. Combined these data indicate that the vast differences in dendritic voltage and calcium transients that occur during the same AP event arise from the nonuniform distribution of A-type K^+ conductance, number of BPs along the path of AP propagation, and minute differences in dendritic diameter between individual branches in the apical tuft.
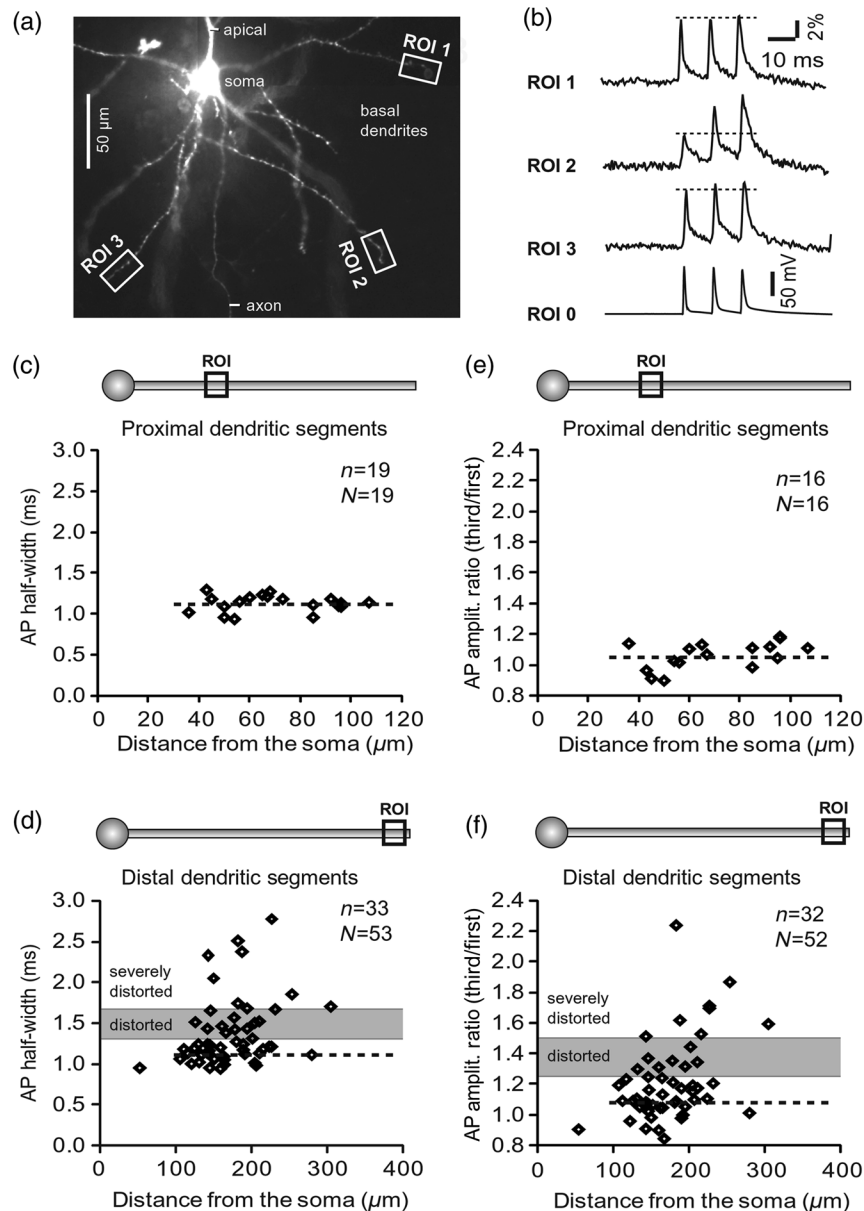

Fig. 1 Heterogeneous action potential (AP) invasion-efficacy in basal dendrites. (a) Layer 5 pyramidal neuron filled with JPW-4090. (b) Voltage-sensitive dye recordings of backpropagating APs obtained at three regions of interest (ROI 1 to 3) are aligned with a whole-cell recording from the cell body (ROI 0). Horizontal dashed line marks the amplitude of the first AP at each sister branch. (c) Cartoon depicts ROI in proximal part of a dendrite. Dashed line indicates the mean AP half-width of 1.06 ms. (d) Cartoon depicts ROI at the tip of a basal dendrite. Dashed line is a copy of the line shown in (c). The bottom edge of the gray area is two standard deviations above the mean obtained in the proximal segments. The top edge of the gray area is five standard deviations above the mean obtained in the proximal segments. The AP voltage waveform is deemed "distorted" if its value lies within the gray area, and "severely distorted" outside the gray area. (e and f) Same as in (c and d), except the Y-axis values are amplitude ratios between third and first spike in AP triplets. n—number of cells; N—number of dendrites.

2 Results

2.1 *AP Propagation Failures in Basal Dendrites*

Voltage-sensitive dye (VSD) imaging method[9] was used to record AP waveforms from the most distal segments of basal branches, dendritic tips [Fig. 1(a), and regions of interest, ROIs 1 to 3]. Simultaneously with optical imaging, the APs were recorded via patch pipette on the cell body [Fig. 1(b), ROI 0]. In the example shown in Fig. 1, AP waveforms were analyzed in three basal branches belonging to the same neuron. In two branches, the half-width of a single-backpropagating AP was similar to that measured in the cell body. During a train of three somatic APs (interspike interval 12.5 ms), the amplitudes of three dendritic spikes were relatively uniform in the most distal segments of two basal branches (Fig. 1, ROI 1 and ROI 3). However, in one sister dendrite, the AP half-width was about twice that obtained in the soma and the amplitude of the first spike in the triplet was less than half that of the third spike (Fig. 1, ROI 2), suggesting a failure of the first AP to invade the distal tip of the basal dendrite. This outcome, the failure of the first AP to invade the dendritic terminal, was detected in five basal dendrites belonging to five pyramidal neurons.

Next, we used the AP half-width as a parameter of the AP invasion efficacy in basal dendrites.[5] VSD recordings of dendritic AP waveforms obtained from proximal dendritic segments at distances ranging from 36 to 107 μm away from the cell body

[Fig. 1(c)] produced AP half-widths clustered around 1 ms (1.13 ± 0.02 ms, mean $\pm$ s.e.m., $n = 19$) clearly indicating that proximal dendritic segments were successfully invaded by backpropagating APs. VSD recordings of dendritic AP waveforms obtained from the most distal segments of 53 basal dendrites in 33 rat PFC L5 pyramidal neurons showed a much wider range of AP half-widths [Fig. 1(d)]. The majority of dendritic AP half-widths fall in a range 1.00 ± 0.25 ms, consistent with previously published measurements.[7,8,10,11] However, a significant number of dendrites (11 out of 53) exhibited distorted AP waveforms with the AP half-width two to five standard deviations greater than the mean established in proximal recordings [Fig. 1(d), gray area]. Moreover, a small group of basal dendrites (10 out of 53) were characterized with severely distorted AP waveforms, more than five standard deviations above the mean [Fig. 1(d), above the gray area], suggesting a failure of the first AP to invade the tips of basal dendrites. The length of a dendritic branch was not the sole determining factor because dendritic segments of similar path distance from the soma (e.g., 200 μm) showed marked heterogeneity in the AP half-width [Fig. 1(d)].

Next, we compared amplitudes of the third and first dendritic spikes in triplets of APs [Fig. 1(b)]. In proximal dendritic segments (<107 μm away from the cell body), the third/first signal amplitude ratio was on average 1.06 ± 0.02 [mean $\pm$ s.e.m., $n = 16$, Fig. 1(e)]. Note that an amplitude ratio around 1.0 indicates successful invasion of the first AP [Fig. 1(b), ROI 1].[5,8] Although the AP amplitude ratios were ∼1.0 in proximal
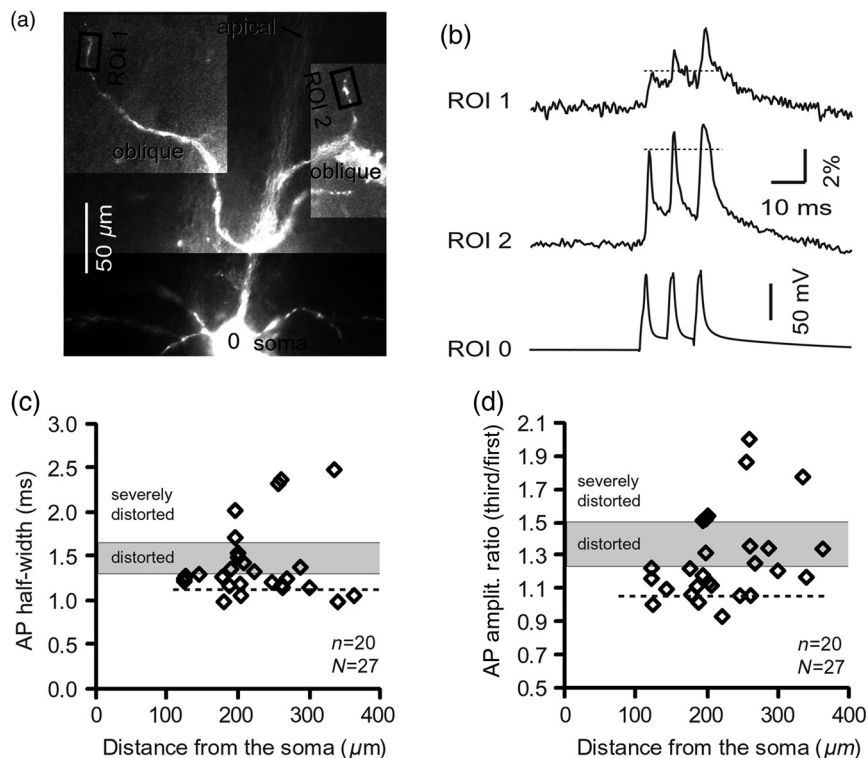

Fig. 2 Heterogeneous AP invasion-efficacy in oblique dendrites. (a) Layer 5 pyramidal neuron filled with JPW-3028. (b) Optical recordings of backpropagating APs obtained from two oblique branches (ROI 1 and ROI 2) are aligned with a whole-cell recording from the cell body (ROI 0). Horizontal dashed line marks the amplitude of the first AP at each sister branch. (c) Scatter plot of AP half-widths obtained from 27 oblique dendrites belonging to 20 pyramidal cells. Dashed horizontal line is the mean AP half-width measured in proximal basal dendrites as shown in Fig. 1(c). Gray rectangle marks two to five standard deviations above the mean AP half-width measured in proximal basal dendrites as shown in Fig. 1(c). (d) Same as in (c) except AP amplitude ratios (third/first) are plotted. The mean and two to five standard deviations are based on proximal basal dendrites (Fig. 1). *n*—number of cells; *N*—number of dendrites.

dendritic segments [Fig. 1(e)], in distal dendritic tips these values were scattered in a markedly wider range [Fig. 1(f)]. A significant number of dendrites exhibited third/first signal amplitude ratios two to five standard deviations above the mean established in proximal segments [Fig. 1(f), gray area]. Moreover, a small group of basal dendrites (8 out of 52) were characterized with severely distorted AP ratios, more than five standard deviations above the mean [Fig. 1(f), above the gray area], suggesting a failure of the first AP to invade the tips of these basal dendrites.

2.2 AP Propagation Failures in Apical Oblique Dendrites

In apical oblique dendrites, such as in basal dendrites, we found sister branches exhibiting highly different voltage profiles under the experimental paradigm involving triplets of APs. In the example shown in Figs. 2(a) and 2(b), two oblique segments in the same cortical layer, belonging to the same L5 pyramidal neuron, exhibit two different levels of AP attenuation and AP amplitude filtering. One oblique dendrite is experiencing three sharp spikes [Fig. 2(b), ROI 2], whereas in the other branch, the first AP is clearly failing [Fig. 2(b), ROI 1]. It is important to state that the AP invasion process is most successful in proximal segments of basal dendrites[7,10] therefore, the properties of AP waveforms established in basal dendrites (Fig. 1) will next be used to gauge AP backpropagation efficacy in the apical oblique tree. The VSD measurements of AP half-widths in apical oblique branches produced values that were overall greater than the mean value (1.13 ms) obtained in proximal segments of basal dendrites [Fig. 2(c), dashed line]. A significant number of "oblique" data points (6 out of 27) fell two to five standard deviations above the 1.13-ms mark [Fig. 2(c), gray area], whereas some points were scattered more than five standard deviations above the mean [Fig. 2(c), above the gray area], suggesting a complete failure of the first spike to invade these oblique branches. Identical conclusions emerged in respect to the third/first spike amplitude ratio in oblique dendrites [Fig. 2(d)]. In summary, the VSD recordings suggested that synaptic contacts near the tips of basal dendrites and apical oblique dendrites experience vastly different voltage depolarizations during single-AP firing, as well as during the first AP in a repetitive firing episode.

2.3 AP Propagation Failures in Apical Tuft Dendrites

AP invasion was studied in apical tuft dendrites of rat PFC L5 pyramidal neurons using calcium imaging.[25,26] All neurons in this experimental group ($n = 18$) were filled with a mixture containing calcium-sensitive dye (OGB1) and a fluorescent probe (AF594) for tracking dendrites [Fig. 3(a)]. Triplets of APs were triggered by somatic current injection via patch pipette with a 120-ms interspike interval (8.3 Hz). AP-associated dendritic Ca^{2+} signals were recorded simultaneously from several sister branches in the visual field [Fig. 3(b)]. In the example shown in Fig. 3, three apical tuft branches experienced vastly different outcomes of AP invasion. The backpropagating AP clearly failed in branch ROI 2 while successfully invading two neighboring branches (ROI 1 and ROI 3) located at the same path distance from the soma. A lack of optical signal in the apical tuft branch ROI 2 could be due to a small signal-to-noise ratio, or it could be due to dendritic injury occurring during slice preparation. In each dendrite with documented failure of AP invasion (6 out of 18 neurons), we were able to test and confirm dendritic viability using a higher frequency of AP firing.[27] In the example shown in Fig. 3, increasing the AP frequency to 50 Hz (20-ms interspike interval) produced robust Ca^{2+} signals in ROI 2 [Fig. 3(d)], thus showing that dendritic branch ROI 2 was normally functioning in the previous trial [Fig. 3(c)]. In summary, these data showed that during an invasion of backpropagating AP into the apical tuft of L5 pyramidal neurons, a subset of dendritic branches do not receive the AP-mediated Ca^{2+} influx despite the fact that at the same moment of time (during the same AP event) the remainder of the apical dendritic tree is amply flushed with Ca^{2+}. In every neuron studied in this way ($n = 18$), we observed significant amplitude differences between dendritic AP-Ca^{2+} in the apical tuft. Large interdendritic differences persisted even after boosting the dendritic Ca^{2+} signals with increased AP frequencies [Fig. 3(d), compare ROI 2 against ROI 3].
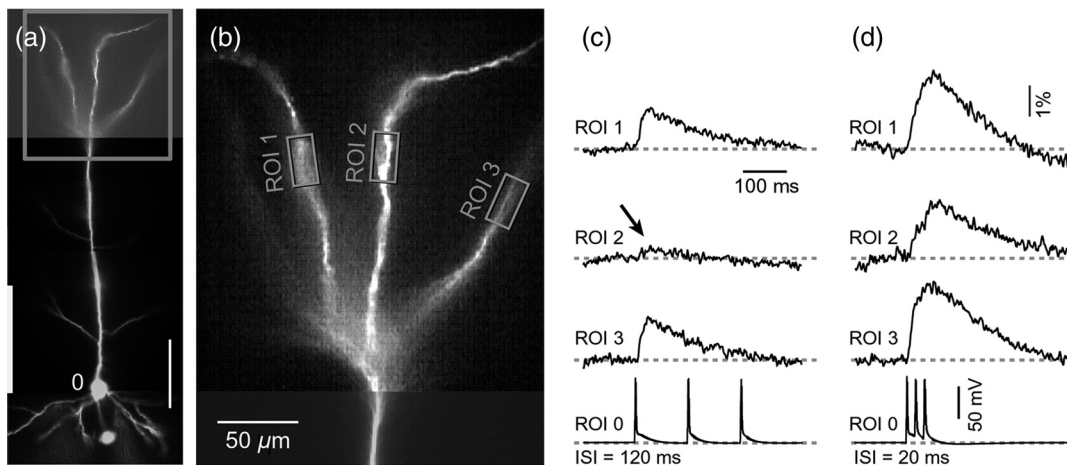

Fig. 3 Branch-specific failure of AP backpropagation into the apical tuft. (a) Layer 5 pyramidal neuron filled with OGB1 and AF594. AF594 channel was used to generate this image. Scale, 100 μm. (b) Blowup of the area marked by the rectangle in (a). (c) Current injections into the soma were used to initiate three APs with interspike interval of 120 ms. Simultaneous recordings of AP-Ca^{2+} signals from three sister branches (ROI 1 to 3) are aligned with the whole-cell recording (ROI 0). Arrow indicates AP failure. (d) Same as in (c), except interspike interval reduced to 20 ms.

2.4 Effect of Dendritic Diameter on the Efficacy of AP Propagation

In order to test whether dendritic diameter affects the efficacy of AP invasion in terminal dendritic branches of the apical tuft, we performed a series of experiments in which optical imaging was followed by morphological analysis. All neurons in this group ($n = 8$) were filled with an internal solution in which a histological stain (biocytin) was added to a mixture of fluorescent dyes OGB1 and AF594. This allowed us to reconstruct pyramidal neurons (in Neurolucida) after the optical imaging session [Fig. 4(a)]. Using a 100× magnification lens, the dendritic diameters were measured in those dendritic segments where optical data were acquired [Fig. 4(b)]. Comparisons between sister branches were performed using a ratio between Ca^{2+} signal amplitudes [Fig. 4(c)] and a ratio between dendritic diameters [Fig. 4(b)]. We found that in an overwhelming majority of the cases (12 out of 15 pairs of sister branches) a branch with a narrower diameter experienced a higher amplitude of the local Ca^{2+} signal than its sister with a larger diameter [Fig. 4(d)].

A paired t-test analysis showed that Ca^{2+} signal amplitudes in thinner branches [Figs. 4(b) and 4(c), ROI 2] were significantly greater ($p = 0.00052$, $N = 15$ pairs) than the Ca^{2+} signal amplitudes in sister branches with larger diameters [Figs. 4(b) and 4(c), ROI 1]. Thinner branches have a higher surface-to-volume ratio (SVR), which may account for the observed higher accumulation of intracellular Ca^{2+} in thinner branches [Fig. 4(d)]. The measured dendritic diameters [Fig. 4(b)] allowed us to calculate SVR for each branch in the pair. In order to "predict" the signal discrepancy based on SVR differences, the SVR of a thinner branch was divided by the SVR of a thicker branch [Fig. 4(e1), SVR_thin/SVR_thick]. This number represents a predicted difference in signal amplitude between two sister branches based solely on their diameters. In the majority of dendritic pairs, both ratios, the one based on experimental measurements (Ca^{2+} amplitude ratio) and the one based on calculations "SVR-ratio," were greater than 1 [Fig. 4(e1)]. However, their exact numerical values were not in agreement [Fig. 4(e1), compare light and dark gray bars]. In fact, linear regression analysis indicated a very poor fit between the values
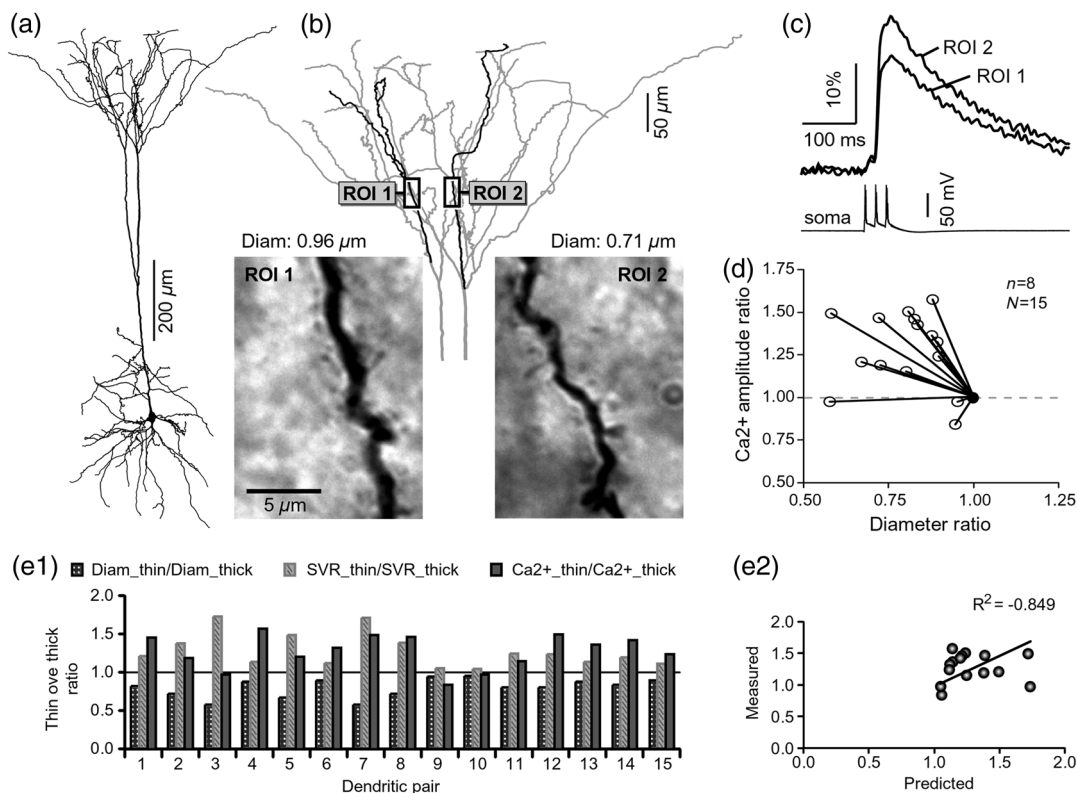

Fig. 4 Thinner branches experience greater AP-Ca^{2+} amplitudes. (a) A layer 5 pyramidal cell filled with OGB1, AF594, and biocytin was reconstructed after the calcium imaging session. (b) Upper: two dendrites (black) were in the same focal plane allowing simultaneous recordings. Lower: 100× magnification lens used to measure dendritic diameters. (c) Current injections into the soma were used to initiate three APs with interspike interval of 20 ms. Simultaneous recordings of dendritic AP-Ca^{2+} signals at two locations marked in (b). (d) Diameters of sister branches in each pair were normalized against the branch with greater diameter (x axis). AP-Ca^{2+} signal amplitudes were normalized against the stronger branch in a pair (y axis). Sister branch pairs are connected by straight lines. Note that AP-Ca^{2+} signal amplitudes were regularly greater in thinner branches. (e1) Each dendritic pair ($N = 15$) is represented by three values: (i) diameter of thinner branch divided by diameter of thicker branch (dotted bar), (ii) calculated surface-to-volume ratio (SVR) of thinner branch divided by calculated SVR of thicker branch (light gray bar), and (iii) measured Ca^{2+} signal in thinner branch divided by Ca^{2+} signal in thicker branch (dark gray bar). Note that in sister branches with similar dendritic diameters (diameter ratio = 1), as determined in dendritic pair #9 or dendritic pair #10, the AP-induced Ca^{2+} transients were very similar, too (Ca^{2+} Ratio = 1). (e2) The measured value (Ca^{2+}_thin/Ca^{2+}_thick) is plotted against the predicted value (SVR_thin/SVR_thick) for each dendritic pair ($N = 15$). Linear regression (forced through zero) has a negative R^2.

predicted from calculating SVR ratios and the measured Ca^{2+} signal amplitude ratios [Fig. 4(e2)], suggesting that factors other than SVR influenced the reported differences in Ca^{2+} amplitudes between sister branches during the same AP event. Those additional factors may include a difference in endogenous calcium buffers between two sister branches (less likely) and a difference in voltage gated channels (more likely).

2.5 Modeling AP-Ca^{2+} Signals in the Apical Tuft

Multicompartmental models are useful tools for analyzing multisite data and for generating a testable hypothesis.[7,10,13,28] We used a reconstructed PFC L5 pyramidal cell [Fig. 5(a)] to test the variability of AP-induced dendritic depolarizations in the apical tuft. A-type voltage-gated potassium conductance (K_A) populates dendrites of pyramidal neurons and opposes AP propagation into the dendritic tree.[29] At one end of the parameter range, we set a uniform density of K_A so that dendritic AP waveforms were large in amplitude and fast in dynamics [Fig. 5(b), A-type = 250 pS/μm^2]. On the end of the parameter range, we adjusted a uniform K_A density so that dendritic AP waveforms were heavily attenuated [Fig. 5(c), A-type = 350 pS/μm^2]. We explored several levels of uniform K_A density in between the two aforementioned extremes. Neither modeling experiment was able to produce large differences in the dendritic AP amplitude between dendritic segments at a similar path distance from the cell body [Figs. 5(b) and 5(c), ROIs 1 to 6]. These data indicate that with a realistic neuronal morphology comprising natural variations in dendritic diameter and uniform density of dendritic K_A conductance, it is rather difficult to create conditions that mimic AP invasion in one and failure in another apical tuft branch [Fig. 3(c)].

2.6 Nonuniform Distribution of A-Type Dendritic Conductance (K_A) Underlies Heterogeneity of Dendritic Excitability among Sister Branches

We next hypothesized that a nonuniform distribution of K_A contributed to the observed heterogeneity in AP invasion of the apical dendrites (Figs. 3 and 4). To test this hypothesis, we endowed one apical tuft branch with a cluster of K_A [Fig. 5(d), gray highlight] while keeping a uniform K_A conductance density (250 pS/μm^2) in the remainder of the dendritic tree. We increased the K_A conductance in the cluster (fivefold, 1250 pS/μm^2) until the backpropagating AP failed to depolarize that the dendritic segment and the difference between the branch with K_A cluster (ROI 6) and a branch without K_A cluster (ROI 1) were pronounced [Fig. 5(e)]. We next hypothesized that a block of K_A conductance with Ba^{2+} (Ref. 30) may remove large differences in AP-Ca^{2+} signals observed between sister branches in real experiments (Figs. 3 and 4). In the modeling experiment, we assumed a 50% efficacy of Ba^{2+}, which resulted in a reduction of global K_A conductance from 250 to 125 pS/μm^2 (50%) and a reduction of local cluster of K_A conductance from 1250 to 625 pS/μm^2 (50%). Following a 50% reduction in K_A conductance [Fig. 5(f)], the two dendritic voltage waveforms exhibited much lesser difference in voltage
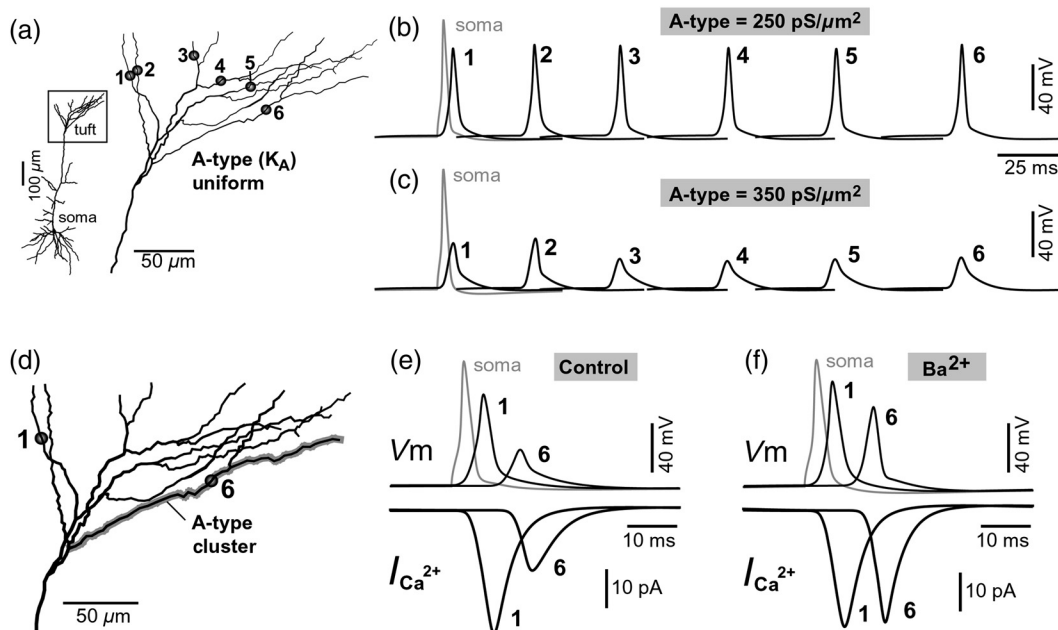

Fig. 5 Modeling AP backpropagation in apical tuft dendrites. (a) Neurolucida reconstructed layer five pyramidal neuron from the rat medial prefrontal cortex (P28). Apical tuft arbor is enlarged with six recording locations (1 to 6) indicated by circles. Current injection into the soma was used to initiate an AP. Sample AP waveforms from the cell body (soma) and sister dendrites 1 to 6 are shown on the right at two levels of global uniform A-type K^+ conductance, (b) 250 pS/μm^2 and (c) 350 pS/μm^2. (d) Apical tuft arbor with two recording locations 1 and 6. Global A-type conductance is 250 pS/μm^2. Gray highlight marks dendritic segments endowed with fivefold higher A-type conductance density than the rest of the apical tuft. Sample AP waveforms from the cell body (soma) and two sister dendrites (1 and 6) are shown before (e) and after (f) application of A-type channel blocker (Ba^{2+}). Calcium currents ($I_{Ca^{2+}}$) in two sister branches are shown below the voltage (Vm) waveforms. Vm and $I_{Ca^{2+}}$ waveforms in sister branch "6" are shifted rightward for clarity. Note that a barium-induced partial block of the global and clustered A-type conductances (50% each) results in equalization of the Ca^{2+} signal in sister branches.

amplitudes, while dendritic Ca^{2+} currents ($I_{Ca^{2+}}$) became very similar [Fig. 5(f), ROIs 1 and 6]. In summary, the modeling data suggested that an abrupt increase in local K_A conductance density (clustering of K_A channels) can reproduce the observed heterogeneity in AP invasion of the apical dendrites (Figs. 3 and 4). The modeling data also suggested that a selective block of neuronal K_A conductance may remove the heterogeneity in AP-Ca^{2+} signals among apical tuft branches.

2.7 Block of A-Type K$^+$ Current (K_A Conductance) causes Stronger Potentiation of AP-Ca^{2+} Signal in the "Weaker" Branch

In the next series of experiments, the model predictions shown in Figs. 5(d)–5(f) were tested in real neurons [Figs. 6(a1) and 6(b1)]. AP-Ca^{2+} signals were recorded simultaneously from several apical tuft branches before and after bath application
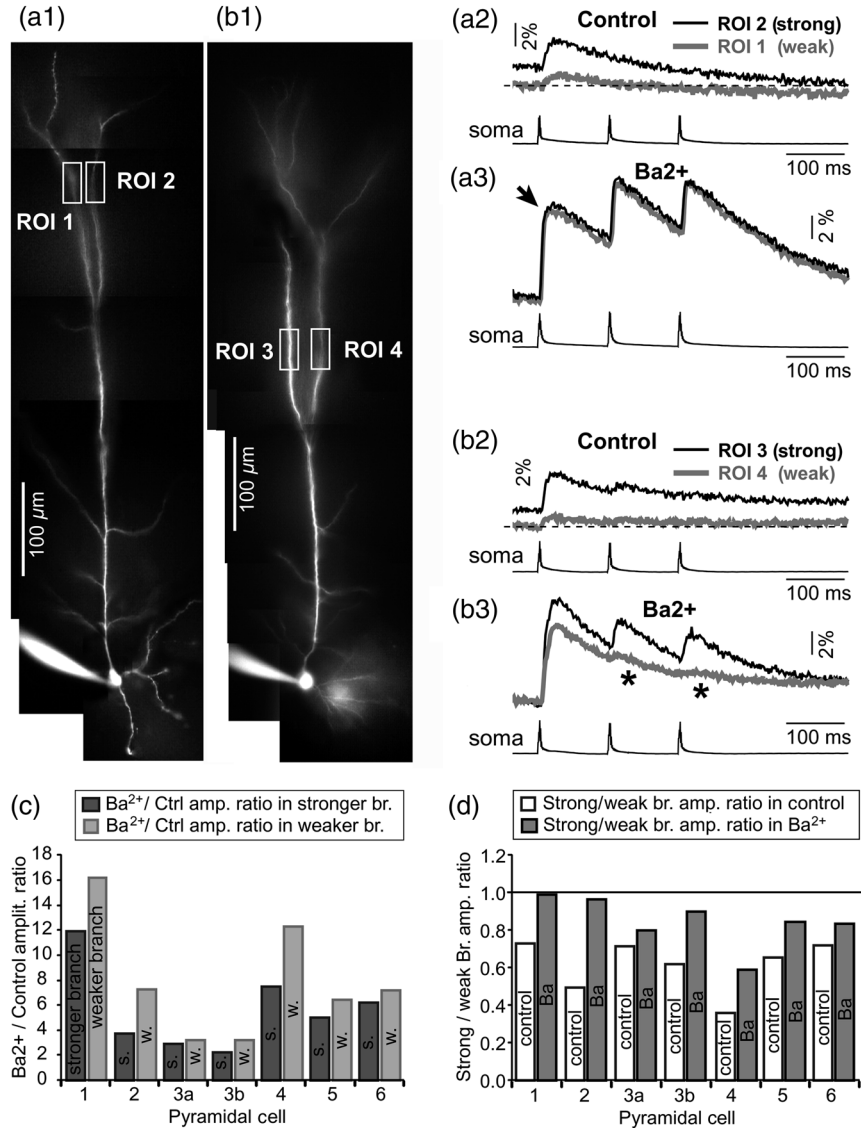

Fig. 6 Block of A-type K$^+$ current causes stronger potentiation of AP-Ca^{2+} signal in the "weaker" branch. (a1 and b1) Two layer five pyramidal neurons filled with OGB1 and AF594. (a2) Upper: current injections into the soma of the cell shown in a1 were used to initiate three APs with an interspike interval of 120 ms. Simultaneous recordings of AP-Ca^{2+} signals from two sister branches (ROI 1 and 2) are aligned with the whole-cell recording (soma). Although positioned at the same path distance from the cell body, the amplitudes of two signals are quite different (hence termed strong and weak). Lower: following application of A-type channel blocker, Ba^{2+} (200 μM), both signals increase in amplitude. The amplitude of the first AP is now nearly identical in both branches (arrow). (b2) Same as in a2, except different cell was used (cell shown in b1). Note that the weaker branch (ROI 4) undergoes several-fold greater potentiation than the stronger branch (ROI 3). Asterisks indicate failed APs in the weaker branch. (c1) Ba^{2+}-induced increase in AP-Ca^{2+} amplitude, expressed as Ba^{2+}/control ratio, was plotted for each of the six cells used in the study. In Cell 3, two pairs of dendrites were studied. In each cell, one pair of branches was studied, as depicted in (a1 and b1). Stronger branches are colored darker gray. Note that the relative potentiation was always stronger in a weaker branch. (c2) Same as in c1 except signal amplitudes were compared between sister branches. Note that block of A-type channels (Ba^{2+}) always reduced the difference between two sisters resulting in a ratio value closer to 1 (dark gray bars).
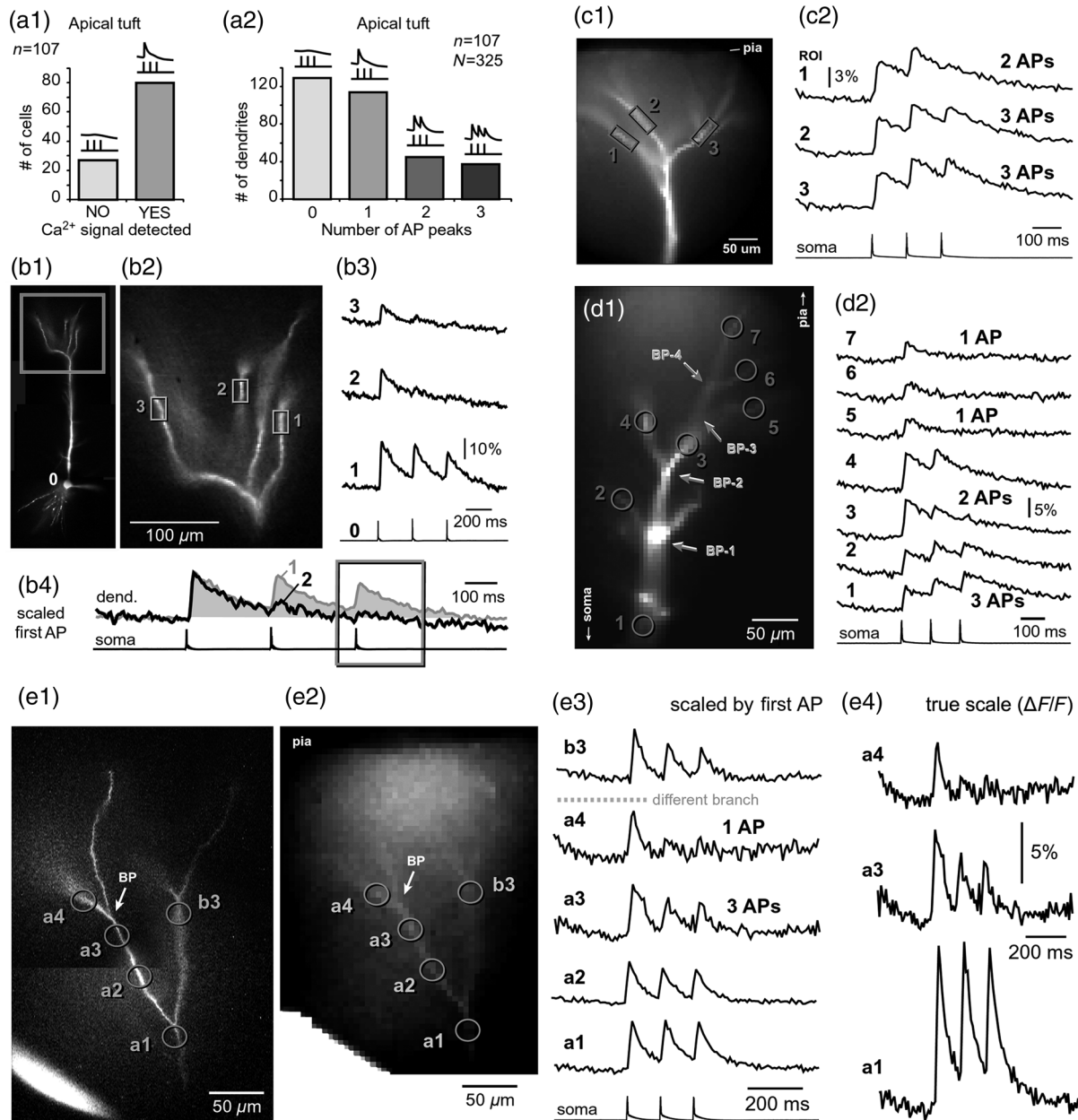
Fig. 7 Differential filtering of backpropagating APs in the apical tuft. (a1) Pyramidal cells in this experimental group ($n = 107$) with signal (YES) or without AP-Ca^{2+} signal detected in apical tuft branches (NO signal). (a2) Apical tuft branches ($N = 325$) are divided based on the number of AP peaks detected (0 to 3). (b1) L5 pyramidal neuron. (b2) Blowup of the area marked by the rectangle in (b1). (b3) Simultaneous recordings of AP-Ca^{2+} signals from three sister branches (ROI 1 to 3) are aligned with the whole-cell recording (ROI 0). (b4) Signals from two branches (ROI 1 and ROI 2) are scaled based on the first AP. Rectangle marks notably different calcium events. (c1) Apical tuft of a L5 pyramidal neuron with three ROIs selected. (c2) One apical tuft branch experiences two APs (ROI 1), while at the same moment of time, other branches experience three APs (ROI 2 and 3). (d1) Apical tuft of a L5 pyramidal neuron with seven ROIs. (d2) Individual branches experience 3, 2, or just 1 AP, depending on the number of branch points (BP) separating them from the main apical trunk. (e1) Apical tuft (AF594 channel) captured by the video microscopy camera. (e2) The same apical tuft (OGB1 channel) captured by the Ca-imaging camera. (e3) Two AP peaks are lost as APs backpropagate through the branch point (BP, arrow)—compare signals before BP (ROI a3) and after propagation through BP (ROI a4). Signals are scaled based on the first AP. (e4) Same data as in (e3), except signal amplitudes are expressed as $\Delta F/F$.

of K$_A$ conductance antagonist Ba^{2+} (200 μM). In control measurements, two sister branches were selected with notably different AP-Ca^{2+} signal amplitudes [Fig. 6(a2)]. A sister branch with a greater AP-Ca^{2+} signal amplitude was named the "stronger branch." Each pair of branches consisted of one strong and one weak branch [Figs. 6(a1) and 6(b1)]. After the Ba^{2+} treatment, the AP-Ca^{2+} signal amplitudes increased drastically in both branches of the strong-weak pair [Figs. 6(a3) and 4(b3)]. In every case without exception, the Ba^{2+}-induced increase in signal amplitude (Ba^{2+}/control ratio) was greater in the weaker

branch than in the stronger branch [Fig. 6(c), $n = 6$ cells, $N = 7$ pairs of dendrites]. We next calculated signal amplitude ratios between the stronger and weaker sisters in two experimental conditions, before (control) and after application of K_A conductance antagonist Ba^{2+} [Fig. 6(d)]. Ba^{2+} treatment removed the difference between strong and weak branches in each pair. The strong/weak amplitude ratio in the Ba^{2+} condition approached the value of 1.0 [Fig. 6(d), dark bars]. In every instance within this experimental group, the blockade of K_A conductance reduced the difference between a strong and weak sister branch in the pair [Fig. 6(d)]. In three cases (Cells 1, 2, and 3b), the difference between strong and weak was almost completely removed, consistent with the modeling result shown in Figs. 5(d)–5(f).

2.8 Branch-Specific and Spike-Order-Specific Filtering of Backpropagating APs

In this experimental series, PFC L5 pyramidal neurons ($n = 107$) were stimulated through somatic patch pipette to produce three APs with an interspike interval of 120 ms. In 27 out of 107 neurons, Ca^{2+} transients were not detected in the apical tuft [Fig. 7(a1), "NO signal"]. In 80 out of 107 cells, the AP-induced Ca^{2+} transients were detected in midsegments of at least one apical tuft branch [Fig. 7(a2), "YES"]. In the entire group of 107 pyramidal cells, a total of 325 apical tuft branches were analyzed for the presence of successful AP invasion. Four types of the AP invasion outcomes were observed. The most common outcome (39.7%) was an apparent lack of any Ca^{2+} transients [Fig. 7(a2), 0 AP peaks detected]. The second most common outcome (35.1%) was a Ca^{2+} signal associated with the first spike only [Fig. 7(a2), "1"]. In 13.8% of branches (45 out of 325), we detected Ca^{2+} peaks associated with first two APs in a train [Fig. 7(a2), "2"]. A one-to-one match between somatic APs and dendritic calcium peaks [Fig. 7(a2), "3"] was detected in only 11.4% of apical tuft branches analyzed in this experimental group (37 out of 325). In 32 out of 107 neurons, the number of Ca^{2+} peaks (successful AP invasions) was not the same in all neighboring apical tuft branches. In the illustrative example shown in Figs. 7(b1)–7(b3), one dendritic branch experiences three APs while two other branches, belonging to the same neuron, experience only one AP at the same instance of time [Fig. 7(b4), rectangle]. In another example, three APs invade apical tuft branches [Figs. 7(c1) and 7(c2), ROI 2 and 3] while only two APs "break" into the neighboring apical tuft dendrite (ROI 1). These data unequivocally show that at the same instance of time two apical tuft branches at an identical path distance from the cell body experience vastly different voltage and Ca^{2+} transients depending on the temporal order of APs in a train.

2.9 APs are Lost at Branch Points

In order to determine the effect of BPs on AP filtering, simultaneous multisite recordings were performed from apical tuft dendrites with multiple branches emanating from parent dendrites [Fig. 7(d1), ROIs 2 to 7]. In this particular example, a backpropagating train of APs crosses four successive BPs on its way from the main apical trunk to the ROI 7 [Fig. 7(d1)]. Optical recordings performed at multiple locations before and after a given BP revealed that the propagation process is shedding off late APs at each BP. More specifically, out of three APs moving from the cell body through ROI 1, only two APs survived the passage through BP-2 and were detected in ROI 3 [Fig. 7(d2)].

Out of two APs detected in ROI 3 only one AP survives the passage through BP-3. From ROI 1 to ROI 7, the backpropagating train of APs travels through four BPs and loses a total of two spikes on this journey. Note that in this particular case, the experimental measurements documented a gradual loss of spikes at each BP location [Fig. 7(d2)]. In some other cases, a train of three spikes [Figs. 7(e1)–7(e3), ROI a2] was swiftly "decimated" to one AP by a single BP [Figs. 7(e1)–7(e3)], compare ROI a3 and ROI a4. The first AP in a train does not pass through a distal BP unhurt. Based on drastic discrepancies in amplitude of the optical signals before and after BP, it can be deduced that even the successful invaders of distal apical tuft are reduced in amplitude [Fig. 7(e4), compare ROI a1 and ROI a4]. The total number of BPs is a very important parameter of AP backpropagation into the apical tuft. A difference as small as just one BP between two AP propagation paths may cause notable differences in the amount of AP filtering at two dendritic locations. In the example shown in Fig. 7(e), one dendritic branch (ROI a4) experiences only one AP, while the neighboring dendritic branch, positioned at a similar path distance from the soma, experiences three APs at the same moment of time [Fig. 7(e3), ROI b3]. One extra BP [Figs. 7(e1) and 7(e2), arrow] is the principal difference between the two propagation processes at ROI a4 and ROI b3. In summary, these data indicate that BPs effectively filter trains of backpropagating APs at a low AP firing frequency ($\sim$10 Hz) by removing later spikes in a train. BPs cut down the number of total spikes invading distal dendritic segments in the apical tufts of L5 pyramidal neurons.

3 Discussion

Optical imaging provides a unique access to cellular compartments too small to tolerate glass electrode recordings.[31,32] Here, we used the basic principles and recording equipment developed by Cohen and Lesher.[33] In the present study, voltage-sensitive and calcium-sensitive dye recordings in basal, apical oblique, and apical tuft dendrites of PFC L5 pyramidal neurons revealed a pronounced heterogeneity of voltage and calcium transients occurring in individual branches at the same distance from the soma and at the same moment of time. Notable differences in dendritic signal dynamics or amplitude were documented among dendritic branches situated in the same cortical layer (two basal, two oblique, or two apical tuft branches) belonging to the same pyramidal cell.

3.1 Voltage Waveforms in Basal and Oblique Dendrites

It was previously shown that the voltage waveforms of backpropagating APs decrease in amplitude with distance from the cell body.[12] At the current state of methodology, the dendritic VSD imaging technique cannot be used to compare signal amplitudes from two locations on the same cell. Despite a linear relation between the optical and electrical signals,[33] the optical signals obtained with internally applied VSDs cannot be calibrated based on a whole-cell recording from the soma. Voltage imaging signal-amplitude, expressed as fractional change in resting light intensity F ($\Delta F/F$), varies along the dendritic tree depending on the exact ratio between the lipophilic membrane experiencing a voltage change (e.g., plasma membrane) and the lipophilic membrane not seeing these membrane potential changes (e.g., internal organelles). Because this membrane ratio varies between neuronal compartments (soma, axon initial segment,

axon, proximal, middle, or distal dendrite) the amplitude of an optical signal in one compartment (e.g., soma) is very different from an optical signal caused by the same voltage change but in a different compartment (e.g., dendrite). As a consequence, voltage imaging cannot be used to determine the amplitude of dendritic AP in millivolts based solely on the somatic whole-cell recording, as discussed in Ref. 7. Actually, absolute values in millivolts can be attained from remote dendrites if voltage imaging is combined with a reliable calibrating signal such as non-attenuating AP[34] or glutamate reversal potential.[35] However, calibration was not attempted here. In the absence of absolute membrane potential values, this project relied on AP shape (half-width) and relative change in AP amplitude within a triplet of APs. Significant increases in AP duration and/or significant changes in relative AP amplitude between subsequent APs are the known signs of altered efficacy of AP propagation or impending AP failure.[5] In contrast to the conclusions of Kampa and Stuart,[5] we found that in the majority of basal dendrites the backpropagating APs invaded the most distal ends of the dendritic branches. In our experiments, there is no uncertainty about the fate of an AP distal to the recording site because in the majority of our measurements the recording site was at the tip of the dendrite (Fig. 1). The discrepancy between our study and that by Kampa and Stuart[5] may simply be because we obtained good signal-to-noise ratios by averaging just four sweeps, while Kampa and Stuart[5] used excessive averaging of up to 100 sweeps. Excessive averaging introduces AP jitter (small variations of the AP latency) and disrupts the shape and amplitude of the briefest signals, which in this case was the first AP [Fig. 1(b)]. No calibration was supplied to determine the amplitude of VSD signals observed in the study of Kampa and Stuart.[5] Both studies, Kampa and Stuart[5] and the present study, rely on relative signal amplitudes, a method previously used in VSD measurements to compare glutamate-mediated dendritic plateau potentials and backpropagating AP in the same segment of a basal dendrite.[36] In general, AP-invasion dichotomy was considered to be an intercellular process, in which two cells of the same class (two hippocampal CA1 pyramidal neurons) exhibit two extreme outcomes of AP backpropagation—invasion and failure.[22] Our recordings of AP voltage waveforms performed on multiple dendrites of the same neuron [Fig. 1(a)] provide unequivocal evidence of an "intracellular" AP-invasion dichotomy. That is, AP invades some but not all dendrites belonging to the same pyramidal cell [Fig. 1(b)]. In summary, systematic VSD imaging revealed a pronounced heterogeneity of AP efficiency in both basal and apical oblique dendrites of PFC L5 pyramidal neurons.

3.2 AP-Induced Dendritic Calcium Signals in the Apical Tuft

Previously published dendritic Ca^{2+} imaging data indicate that single AP (or low-frequency AP train) either failed or succeeded in inducing dendritic Ca^{2+} transients in the apical tuft of cortical pyramidal neurons.[16,23,25,37–40] Half of these studies claimed an apparent failure of a single AP, whereas the other half claimed a successful invasion of distal apical dendrites by a single AP. In the present study, we found evidence to support both views; the failures and the successes. In 25.3% of L5 pyramidal neurons tested in this way, the AP-Ca^{2+} transients were not detected in any branch of the apical tuft [Fig. 7(a)]. In the remaining 74.7% of the cells, clear Ca^{2+} signals were detected in at least one apical tuft branch in response to a single-somatic AP or triplet of

APs at a slow firing rate (<10 Hz). The observed dichotomy of AP backpropagation in pyramidal neurons belonging to one putative class of cells (PFC L5 pyramidal cells) can be attributed to subtle differences in either the diameter of the primary apical dendrite, branching pattern or distribution, density, or modulatory state of voltage-gated channels along the somatodendritic axis,[41] as previously concluded by Golding et al.,[21] who used hippocampal CA1 neurons in their study.[22] Here, we extend the Golding et al. repertoire of dendritic heterogeneities in five directions. First, we confirm the presence of dendritic dichotomy in PFC L5 pyramidal cells. Second, we determined that the smaller diameter apical tuft branches experience a higher amplitude of AP-Ca^{2+} transients than their sister branches in the same cell (Fig. 4). Third, we provide evidence that a nonuniform distribution of A-type K^+ conductance is responsible for the observed heterogeneity among sister branches in the apical tuft (Figs. 5 and 6). Fourth, we reveal differential filtering of AP trains in apical tuft branches, resulting in an unequal number of APs arriving in two neighboring sister branches [Fig. 7(b)]. Fifth, we determined that dendritic BPs cleave off the late spikes in an AP train. As an AP train backpropagates into more and more distal dendritic segments fewer and fewer spikes remain in the train [Fig. 7(d)].

3.3 Branch-Specific AP Invasion Efficacy

The present study revealed that dendritic segments of similar path distance from the soma showed a marked heterogeneity in the amount of Ca^{2+} influx during the same AP event (Fig. 3), consistent with the findings in hippocampal CA1 neurons.[16] Spruston et al.[16] used Ca^{2+} imaging to study sister branches. We used voltage imaging to learn that the voltage waveforms of backpropagating APs exhibit dramatic differences between two or more sister branches belonging to the same cell. This is a surprising finding in basal dendrites given their relatively short path distance from the cell body and the fact that a significant portion of dendritic depolarization comes from a passive spread of voltage from the soma into a basal dendrite.[7,13,38] Previous publications stated that APs fail to invade basal dendrites[5,6] implicating a robust physiological principle applicable to all basal dendrites in one pyramidal neuron. New data clearly showed that basal dendrites cannot be considered as a monolith compartment with a predictable excitability profile. Although some basal dendrites receive little depolarization during low frequency firing, a significant number of basal dendrites are successfully invaded by backpropagating AP, as evident from Ca^{2+} imaging,[7,8] and voltage imaging[8,11] of the most distal segments on these basal dendrites.

Apical oblique branches were traditionally studied by Ca^{2+} imaging,[30] while the voltage waveforms of backpropagating APs in apical oblique dendrites were not readily available, but see Refs. 7 and 42. The present study revealed that the same type of the AP-invasion uncertainty found in the basilar dendritic tree also exists in apical oblique branches of PFC L5 pyramidal neurons (Fig. 2). Therefore, the apical oblique dendrites cannot be considered as a monolith, gradually changing compartment, with a predictable excitability profile, solely dependent on the path distance from the soma. Instead, some oblique branches receive small, while other oblique branches, belonging to the same neuron, receive large depolarizations during low frequency AP firing.

3.4 Order-Specific AP Invasion Efficacy

At AP firing frequencies smaller than 10 Hz, individual apical tuft branches belonging to the same neuron, develop highly heterogeneous voltage profiles. At identical path distances from the soma, two dendritic segments positioned on two neighboring apical tuft branches experience dramatically different outcomes of AP invasion. In the present project, high sampling rates (200 to 500-Hz frame rate) allowed us to detect Ca^{2+} peaks corresponding to each AP in the train (Fig. 7), whereas a multi-site approach allowed us to compare Ca^{2+} peaks in two or more apical tuft dendrites occurring at the same moment of time. The dichotomy between apical tuft branches described in Fig. 3(c) was based on the passage or failure of the first AP in the train of APs. However, even in the case in which the first AP invaded both apical tuft branches, the AP backpropagation process still had notably different outcomes for later spikes in a train.[43] Our recordings showed that the number of AP-Ca^{2+} peaks in any given apical branch varied between 0, 1, 2, and 3 [Fig. 7(a2)]. For example, one apical branch was invaded with all three spikes in a train, whereas in the neighboring branch only the first AP was successful [Fig. 7(b)].

Failing APs bring negligible Ca^{2+} into dendrites (Fig. 3), therefore, it is highly possible that Ca^{2+}-dependent dendritic processes would undertake completely different paths in two neighboring apical tuft branches during the same episode of neuronal electrical activity [Fig. 7(f)]. Based on the rules of STDP, the synaptic inputs coinciding with the second and third spikes in a train will potentiate in one and depress in another branch of the same pyramidal neuron at the same moment of time. Complex scenarios for synaptic plasticity rules in neurons with long dendrites (cortical pyramidal neurons) have been proposed in the past. Some of these rules were based on the absolute distance between the synaptic input site and the soma.[44–47] These studies implicate that synaptic inputs arriving in different cortical layers are subject to different learning rules.[44,45] Here, we unequivocally show that two synaptic inputs converging into the same cortical layer (layer 5 = basal dendrites; layer 4 = oblique dendrites; layer 1 = apical tuft dendrites), and arriving on the same pyramidal neuron, at the same distance from the cell body, encounter dramatically different dendritic voltage and calcium transients (Figs. 1–3). Therefore, the layer specificity of synaptic inputs may not be a good predictor of excitatory postsynaptic potential–AP interactions.

3.5 Intraneuronal Functional Maps can be Very Complex

Several functional parameters that are known to possess orderly gradients within a single neuron[29,48] have prompted a notion of intraneuronal topographic functional maps. Narayanan and Johnston[49] define a functional map within a neuron as an orderly progression of a functional parameter on the topography of the neuron. A functional map, as depicted in Fig. 1 of Ref. 49, may apply to the thick apical trunk, but it does not apply to thin dendrites (oblique and tuft) according to our new experimental data. Individual dendrites, branching off the main apical trunk (oblique and tuft dendrites), possess unique, highly divergent, branch-specific properties (Figs. 1–7), which cannot be predicted from the generalized spatial distributions of dendritic voltage-gated conductances (Fig. 1 of Ref. 49).

3.6 Mechanisms of AP Heterogeneity in Sister Dendrites

Although it is entirely obvious that passive[22,50,51] and active dendritic properties[29,48,52–54] may underlie the difference in AP backpropagation efficacy between proximal and distal dendritic regions,[24,37,38,40,55] it is considerably more difficult to understand why two daughter branches stemming from the same parent dendrite, at a similar path distance from the soma, exhibit highly variable voltage and calcium dynamics during the same AP backpropagation event (Fig. 3).[16,56] Three major factors determine the success or the failure of an AP to invade an apical tuft branch. The first factor is the diameter of a daughter branch. AP propagates (backpropagates) from a thick apical trunk (parent) into several thin apical tuft branches (daughters). The effect of a variable cable diameter on the propagation of regenerative membrane potentials was thoroughly dissected in the classical works of neuro-biophysics.[50,57,58] Briefly, the daughter branches with smaller diameters are endowed with greater input impedance, and therefore, present lesser obstacle for an AP emanating from the parent dendrite than daughter branches with larger diameters (Fig. 4). This theoretical conclusion is supported by our current data, as Ca^{2+} signal amplitudes were always greater in thinner branches [Fig. 4(d)]. However, the greater Ca^{2+} signal in the thinner branch can also be explained by a more favorable SVR in the thinner branch [Fig. 4(e1), light gray bars]. Due to this inherent sensitivity of the Ca^{2+} signal to SVR, the current data cannot be used to conclude that the observed differences in Ca^{2+} signal amplitudes (Figs. 3 and 4) were caused by greater voltage depolarizations (stronger AP invasion). Nevertheless, the current data clearly established that thinner branches do experience substantially greater Ca^{2+} signal amplitudes during the same AP event [Figs. 4(d) and (e1)]. The second factor which determines the extent of AP invasion is a nonuniform distribution of A-type dendritic conductance (Fig. 5). Fast-activating A-type K^+ channels act to prevent large, rapid dendritic depolarizations, thereby regulating orthograde and retrograde propagation of dendritic potentials in CA1 pyramidal cells.[29,59] As in hippocampus, these channels effectively prevent and limit the backpropagation of APs into the basal, oblique, and apical dendrites of neocortical pyramidal neurons too.[10,29,30,60] The modeling experiments (Fig. 5) showed that naturally occurring differences in the daughter branch diameter can only account for small but not large differences in AP-Ca^{2+} amplitudes between two apical tuft sisters. The first AP in a low frequency train is a biophysical equivalent of a single AP. As slow voltage-gated dendritic currents (h-current and Ca^{2+}-currents) have a minimal impact on a single AP, a differential invasion of the first AP in a train [Fig. 3(c)] can be achieved by combining the daughter diameter with a nonuniform distribution of fast voltage-gated dendritic conductances (Na^+ or K^+). There is little evidence of variations in dendritic Na^+ conductance density along a dendrite,[14] and if experimental data do sometimes point to a nonuniform distribution of dendritic Na^+ channels, the gradients of conductance with distance from the cell body are very shallow.[6,10] The story of the A-type K^+ membrane conductance, on the other hand, is laid with examples of highly nonuniform channel distributions.[10,60–65] Our computational model explored the effect of a K_A channel cluster in apical tuft branches. The modeling data indicated that sister branches carrying clusters of A-type channels would show a greater rate of single-AP failures than the neighboring sister branches without such clusters [Fig. 5(e)]. The modeling data

indicated that a selective block of A-type channels would effectively eliminate differences in voltage and calcium transients between the tuft sisters [Fig. 5(f)]. This model prediction was confirmed in real experiments using an A-type channel antagonist (Fig. 6). Combined modeling and pharmacology experiments (Figs. 5 and 6) suggest that in straight dendrites with fewer BPs, A-type channels are responsible for a highly heterogeneous nature of AP invasion into the sister branches of the apical tuft. In conclusion, the observed large differences in AP-Ca^{2+} amplitudes between two apical tuft sister branches seem to depend on the total number of BPs [Figs. 7(d) and 7(e)], dendritic diameter (Fig. 4) and nonuniform distribution of A-type K^+ channels in the membrane.

4 Summary

Branch-specific invasion of the AP (Figs. 1–3) and branch-specific filtering of AP trains (Fig. 7) strongly indicate that a feedback AP signal (backpropagating AP) interacts with synaptic contacts in a manner that cannot be predicted from the generalized spatial distributions of passive and active dendritic properties obtained from patch electrode recordings along the thick apical trunk. The focus of the current project was on fine (thin) dendritic branches, basal oblique, and tuft dendrites. During an episode of slow (<10 Hz) AP firing (triplet of APs with 120-ms interspike interval) some of these thin dendrites receive 0 spikes, some receive just one spike, while others experience two or even all three spikes in a train. An orderly progression of a functional parameter on the topography of a neuron (Fig. 1 of Ref. 49) [Acker and Antic,[10] their Figs. 7(a) and 7(b)] cannot be used to precisely describe signal integration in real neurons because dendritic segments belonging to the same class of dendrites (basal, oblique, or tuft), positioned at the same path distance from the soma experience vastly different voltage and calcium transients at the same moment of time. Synaptic inputs seeking robust coupling with the axonal output (AP initiation site) must not only choose an appropriate cortical layer and an appropriate pyramidal cell, but more importantly they must "choose" a specific dendritic branch. The heterogeneity of AP invasion efficacies among two seemingly equivalent sister branches (two basal, two oblique, and two apical tuft dendrites) probably serves to increase the complexity of signal integrations at the level of an individual neuron, to expand the list and range of neuronal parameters eligible for modulatory/plastic changes, and to further reduce the deterministic aspect while increasing the stochastic nature of cortical processing.[66] Paradoxically, information processing is not only dependent on signal strength but also on a certain amount of basic noise and randomness.[67–69]

5 Methods

5.1 Brain Slice and Electrophysiology

Sprague-Dawley rats (P21–42) were anaesthetized with isoflurane inhalation, decapitated, and the brains extracted with the head immersed in ice-cold, artificial cerebrospinal fluid (ACSF), according to an animal protocol approved by the Center for Laboratory Animal Care, University of Connecticut. ACSF contained (in millimeters): 125 NaCl, 26 NaHCO₃, 10 glucose, 2.3 KCl, 1.26 KH₂PO₄, 2 CaCl₂, and 1 MgSO₄, pH 7.4. Coronal slices (300 μm) were cut from frontal lobes. All experimental measurements were performed at 32°C to 34°C. Whole-cell recordings were made from visually identified layer five pyramidal neurons within the medial PFC, including prelimbic and infralimbic cortex. Intracellular solution contained (in millimeters): 135 potassium gluconate, 2 $MgCl_2$, 3 Na_2-ATP, 10 Na_2-phosphocreatine, 0.3 Na_2-GTP, and 10 Hepes (pH 7.3). Electrical signals were amplified with a Multiclamp 700B and digitized with two input boards: (1) Digidata Series 1322 A (Molecular Devices, Union City, California) and (2) Neuroplex (RedShirtImaging, Decatur, Georgia). Only cells with a membrane potential more negative than −50 mV (not corrected for junction potential) and AP amplitudes exceeding 80 mV (measured from the baseline) were included in this study. APs were evoked with depolarizing current steps injected into the cell body (intensity 1.0 to 1.5 nA; duration 1.5 to 2.0 ms).

5.2 Dye Injection

VSD (JPW-3028, provided by Leslie Loew, UConn Health)[70] and calcium-sensitive dye (Oregon Green BAPTA-1, OGB1, Invitrogen) were dissolved in intracellular solution. The protocol for VSD injection was previously described in Ref. 7. Briefly, neurons were filled through whole-cell patching pipettes with JPW-3028. Loading pipettes were filled with two varieties of the same intracellular solution, one with and one without the dye. Dye-free solution was occupying the tip of the pipette, while the back of the pipette lumen was loaded with dye-rich solution (400 to 800 μM). The purpose of dye-free solution in the pipette tip was to prevent dye-leak during the maneuver through brain slice tissue. This procedure is considerably less important for calcium-sensitive dye injection. JPW3028 was injected at room temperature for 30 to 45 min. The filling pipette was carefully pulled out (outside-out patch) and brain slices were left to incubate for 2 to 3 h at room temperature. Right before optical recordings, the cells were re-patched with a dye-free pipette at (32°C to 34°C). In calcium imaging experiments, Alexa Fluor 594, AF594 (80 μM) was included in the intracellular solution to aid the positioning of dendrites inside the camera visual field. The calcium-sensitive dyes were injected for 30 to 45 min before optical recordings.

5.3 Dendritic Voltage and Calcium Imaging

Multisite dendritic imaging was performed on an Olympus BX51WI microscope equipped with a 40× objective, two camera ports and a low-ripple light source for epi-illumination—Xenon arc lamp (OptiQuip, Highland Mills, New York). Functional dendritic imaging was performed with a NeuroCCD camera (80 × 80 pixels, RedShirtImaging, LLC, Decatur, Georgia). Voltage and calcium signals were sampled at a 2000 or 200 Hz frame rate, respectively. Optical filters were from Chroma Technology (Rockingham, Vermont) and Omega Optical (Brattleboro, Vermont). The filters for Alexa Fluor 594 were Chroma exciter HQ580/20×, dichroic Q595LP, and emitter HQ630/60m. The filters for Oregon Green Bapta-1 contained Omega exciter 500AF25, dichroic 525DRLP, and emitter 530ALP. The filter set for voltage-imaging (JPW-3028) consisted of Chroma exciter D510/60, dichroic 570dcxru, and emitter E600lp. A spike-triggered averaging routine available in Neuroplex (RedShirtImaging, Decatur, Georgia) was used to improve the quality of measurements (signal-to-noise ratio).

5.4 Data Analysis

Analysis of optical data, including spatial averaging, high pass filtering, and low pass filtering, was conducted with Neuroplex

8.0.0 (RedShirtImaging, LLC). To process off-line calcium imaging data, we applied a Butterworth high pass filter at a 0.1-Hz cut-off and a Gaussian low pass filter at a 90-Hz cut-off; for voltage imaging processing, the high and low pass filters were set at Butterworth 1 Hz and Gaussian 900 Hz unless otherwise specified. Electrical recordings were analyzed in AxoScope9.2 (Axon Instruments, Inc.).

Statistical tests were performed using SigmaPlot 8.02. All statistics were done on raw data points before normalization. Paired student's t-test was used for comparing data obtained from sister branches belonging to the same neuron. Significance was set as p value <0.05 and high significance as $p < 0.01$. Values are presented as mean $\pm$ s.e.m.. In the calculation of the SVR, dendritic segments were treated as right circular cylinders. The lateral surface of a dendritic segment equals to $D \cdot \pi \cdot L$, where "D" is the dendritic diameter, and "L" is the length of the dendritic segment. The volume equals to $(D/2)^2 \cdot \pi \cdot L$. Hence, $SVR = 4/D$. If the Ca^{2+} signal size depends on SVR only, then one can predict the difference between two branches based solely on dendritic diameters. In other words, the SVR of a thin branch divided by the SVR of the thick branch (SVR_thin/SVR_thick) should match the ratio "Ca^{2+}_thin/Ca^{2+}_thick".

5.5 Model Simulation

Simulations were performed in NEURON (Ref. 71). The model cell was based on a biocytin-reconstructed PFC layer 5 pyramidal cell. The morphology with incorporated voltage-gated channels is copied from[10] and available in ModelDB (Ref. 72). Voltage-gated sodium channels were distributed on the model's soma, axon, and apical dendrites with maximal conductance densities of 900, 5000, and 100 pS/μm^2, in each region, respectively. The large axonal sodium conductance was used for robust axonal AP initiation. Delayed rectifier potassium channel conductance density was 40 pS/μm^2 except in the model's axon, where it was 100 pS/μm^2. In the soma, A-type potassium channels of the "proximal" type[73] were added with a conductance density of 150 pS/μm^2. In the apical dendrites, the distal A-type potassium conductance density was set uniformly at 350 pS/μm^2 and varied between trials in the range from 250 to 350 pS/μm^2. The axon included a low-threshold activated, slowly inactivating potassium current with a conductance density of 50 pS/μm^2 beyond a 15-μm distance from the soma. A low-threshold voltage-dependent calcium conductance was distributed on the dendrites (locations ≥ 30 μm from the soma) with a conductance density of 1.6 pS/μm^2 along with a high-voltage-activated calcium conductance at 0.4 pS/μm^2. The soma and perisomatic regions contained 8 and 2 pS/μm^2 of low-threshold and high-voltage-activated calcium conductance, respectively. Passive membrane properties were as follows: specific intracellular resistivity = 90 $\Omega \cdot$ cm, specific membrane capacitance = 1 μF/cm^2, leak conductance = 0.04 mS/cm^2. To account for dendritic spines, a "spine factor" of 1.5 was used to increase capacitance and leak conductance in the dendrites beyond a distance of 50 μm.

References

1. G. Stuart, J. Schiller, and B. Sakmann, "Action potential initiation and propagation in rat neocortical pyramidal neurons," *J. Physiol. (Lond.)* **505**(Pt 3), 617–632 (1997).
2. H. Markram et al., "Regulation of synaptic efficacy by coincidence of postsynaptic APs and EPSPs," *Science* **275**(5297), 213–215 (1997).
3. J. C. Magee and D. Johnston, "A synaptically controlled, associative signal for Hebbian plasticity in hippocampal neurons," *Science* **275**(5297), 209–213 (1997).
4. N. Spruston, "Pyramidal neurons: dendritic structure and synaptic integration," *Nat. Rev. Neurosci.* **9**(3), 206–221 (2008).
5. B. M. Kampa and G. J. Stuart, "Calcium spikes in basal dendrites of layer 5 pyramidal neurons during action potential bursts," *J. Neurosci.* **26**(28), 7424–7432 (2006).
6. T. Nevian et al., "Properties of basal dendrites of layer 5 pyramidal neurons: a direct patch-clamp recording study," *Nat. Neurosci.* **10**(2), 206–214 (2007).
7. S. D. Antic, "Action potentials in basal and oblique dendrites of rat neocortical pyramidal neurons," *J. Physiol.* **550**(1), 35–50 (2003).
8. W. L. Zhou et al., "Dynamics of action potential backpropagation in basal dendrites of prefrontal cortical pyramidal neurons," *Eur. J. Neurosci.* **27**(4), 1–14 (2008).
9. W. L. Zhou et al., "Intracellular long wavelength voltage-sensitive dyes for studying the dynamics of action potentials in axons and thin dendrites," *J. Neurosci. Methods* **164**(2), 225–239 (2007).
10. C. D. Acker and S. D. Antic, "Quantitative assessment of the distributions of membrane conductances involved in action potential backpropagation along basal dendrites," *J. Neurophysiol.* **101**(3), 1524–1541 (2009).
11. K. P. Holthoff, D. P. Zecevic, and A. Konnerth, "Rapid time-course of action potentials in spines and remote dendrites of mouse visual cortex neurons," *J. Physiol.* **588**(7), 1085–1096 (2010).
12. G. J. Stuart and B. Sakmann, "Active propagation of somatic action potentials into neocortical pyramidal cell dendrites," *Nature* **367**(6458), 69–72 (1994).
13. M. Rapp, Y. Yarom, and I. Segev, "Modeling back propagating action potential in weakly excitable dendrites of neocortical pyramidal cells," *Proc. Natl. Acad. Sci. U. S. A.* **93**(21), 11985–11990 (1996).
14. J. C. Magee and D. Johnston, "Characterization of single voltage-gated Na$^+$ and Ca^{2+} channels in apical dendrites of rat CA1 pyramidal neurons," *J. Physiol. (Lond)* **487**(Pt 1), 67–90 (1995).
15. Y. Manor, C. Koch, and I. Segev, "Effect of geometrical irregularities on propagation delay in axonal trees," *Biophys. J.* **60**(6), 1424–1437 (1991).
16. N. Spruston et al., "Activity-dependent action potential invasion and calcium influx into hippocampal CA1 dendrites," *Science* **268**(5208), 297–300 (1995).
17. G. Q. Bi and M. M. Poo, "Synaptic modifications in cultured hippocampal neurons: dependence on spike timing, synaptic strength, and postsynaptic cell type," *J. Neurosci.* **18**(24), 10464–10472 (1998).
18. P. J. Sjostrom et al., "Dendritic excitability and synaptic plasticity," *Physiol. Rev.* **88**(2), 769–840 (2008).
19. D. E. Feldman, "The spike-timing dependence of plasticity," *Neuron* **75**(4), 556–571 (2012).
20. I. Llano, Y. P. Tan, and C. Caputo, "Spatial heterogeneity of intracellular Ca^{2+} signals in axons of basket cells from rat cerebellar slices," *J. Physiol.* **502**(Pt 3), 509–519 (1997).
21. H. J. Koester et al., "Calcium dynamics associated with action potentials in single nerve terminals of pyramidal cells in layer 2/3 of the young rat neocortex," *J. Physiol. (Lond)* **529**, 625–646 (2000).
22. N. L. Golding, W. L. Kath, and N. Spruston, "Dichotomy of action-potential backpropagation in CA1 pyramidal neuron dendrites," *J. Neurophysiol.* **86**(6), 2998–3010 (2001).

23. F. Helmchen et al., "In vivo dendritic calcium dynamics in deep-layer cortical pyramidal neurons," *Nat. Neurosci.* **2**(11), 989–996 (1999).

24. M. E. Larkum, J. J. Zhu, and B. Sakmann, "Dendritic mechanisms underlying the coupling of the dendritic with the axonal action potential initiation zone of adult rat layer 5 pyramidal neurons," *J. Physiol. (Lond)* **533**(2), 447–466 (2001).

25. D. B. Jaffe et al., "The spread of Na^+ spikes determines the pattern of dendritic Ca^{2+} entry into hippocampal neurons," *Nature* **357**(6375), 244–246 (1992).

26. N. Lasser-Ross et al., "High time resolution fluorescence imaging with a CCD camera," *J. Neurosci. Methods* **36**(2–3), 253–261 (1991).

27. M. E. Larkum, K. M. Kaiser, and B. Sakmann, "Calcium electrogenesis in distal apical dendrites of layer 5 pyramidal cells at a critical frequency of back-propagating action potentials," *P.N.A.S.* **96**(25), 14600–14604 (1999).

28. G. Stuart and N. Spruston, "Determinants of voltage attenuation in neocortical pyramidal neuron dendrites," *J. Neurosci.* **18**(10), 3501–3510 (1998).

29. D. A. Hoffman et al., "K^+ channel regulation of signal propagation in dendrites of hippocampal pyramidal neurons," *Nature* **387**(6636), 869–875 (1997).

30. S. Gasparini et al., "Associative pairing enhances action potential back-propagation in radial oblique branches of CA1 pyramidal neurons," *J. Physiol.* **580**(3), 289–302 (2007).

31. B. M. Salzberg et al., "Measuring intrinsic optical signals from Mammalian nerve terminals," *Cold Spring Harb. Protoc.* **2012**(12), 1273–1279 (2012).

32. M. Canepari et al., "Combining Ca^{2+} and membrane potential imaging in single neurons," *Cold Spring Harb. Protoc.* **2013**(12), 1161–1164 (2013).

33. L. B. Cohen and S. Lesher, "Optical monitoring of membrane potential: methods of multisite optical measurement," *Soc. Gen. Physiol. Ser.* **40**, 71–99 (1986).

34. M. Djurisic et al., "Voltage imaging from dendrites of mitral cells: EPSP attenuation and spike trigger zones," *J. Neurosci.* **24**(30), 6703–6714 (2004).

35. K. E. Vogt et al., "Combining membrane potential imaging with L-glutamate or GABA photorelease," *PLoS One* **6**(10), e24911 (2011).

36. B. A. Milojkovic et al., "Burst generation in rat pyramidal neurones by regenerative potentials elicited in a restricted part of the basilar dendritic tree," *J. Physiol.* **558**(1), 193–211 (2004).

37. J. Waters et al., "Supralinear Ca^{2+} influx into dendritic tufts of layer 2/3 neocortical pyramidal neurons in vitro and in vivo," *J. Neurosci.* **23**(24), 8558–8567 (2003).

38. J. Schiller, F. Helmchen, and B. Sakmann, "Spatial profile of dendritic calcium transients evoked by action potentials in rat neocortical pyramidal neurones," *J. Physiol. (Lond)* **487**(Pt 3), 583–600 (1995).

39. A. T. Gulledge and G. J. Stuart, "Action potential initiation and propagation in layer 5 pyramidal neurons of the rat prefrontal cortex: absence of dopamine modulation," *J. Neurosci.* **23**(36), 11363–11372 (2003).

40. A. M. Barth et al., "Alpha2-adrenergic receptors modify dendritic spike generation via HCN channels in the prefrontal cortex," *J. Neurophysiol.* **99**(1), 394–401 (2008).

41. H. Tsubokawa and W. N. Ross, "Muscarinic modulation of spike back-propagation in the apical dendrites of hippocampal CA1 pyramidal neurons," *J. Neurosci.* **17**(15), 5782–5791 (1997).

42. M. Canepari, M. Djurisic, and D. Zecevic, "Dendritic signals from the rat hippocampal CA1 pyramidal neurons during coincident pre- and post-synaptic activity: a combined voltage- and calcium-imaging study," *J. Physiol.* **580**(Pt 2), 463–484 (2007).

43. J. C. Callaway and W. N. Ross, "Frequency-dependent propagation of sodium action potentials in dendrites of hippocampal CA1 pyramidal neurons," *J. Neurophysiol.* **74**(4), 1395–1403 (1995).

44. P. J. Sjostrom and M. Hausser, "A cooperative switch determines the sign of synaptic plasticity in distal dendrites of neocortical pyramidal neurons," *Neuron* **51**(2), 227–238 (2006).

45. R. C. Froemke, M. M. Poo, and Y. Dan, "Spike-timing-dependent synaptic plasticity depends on dendritic location," *Nature* **434**(7030), 221–225 (2005).

46. B. M. Kampa, J. J. Letzkus, and G. J. Stuart, "Requirement of dendritic calcium spikes for induction of spike-timing-dependent synaptic plasticity," *J. Physiol.* **574**(1), 283–290 (2006).

47. U. Gordon, A. Polsky, and J. Schiller, "Plasticity compartments in basal dendrites of neocortical pyramidal neurons," *J. Neurosci.* **26**(49), 12717–12726 (2006).

48. J. C. Magee, "Dendritic hyperpolarization-activated currents modify the integrative properties of hippocampal CA1 pyramidal neurons," *J. Neurosci.* **18**(19), 7613–7624 (1998).

49. R. Narayanan and D. Johnston, "Functional maps within a single neuron," *J. Neurophysiol.* **108**(9), 2343–2351 (2012).

50. S. S. Goldstein and W. Rall, "Changes of action potential shape and velocity for changing core conductor geometry," *Biophys. J.* **14**(10), 731–757 (1974).

51. P. Vetter, A. Roth, and M. Hausser, "Propagation of action potentials in dendrites depends on dendritic morphology," *J. Neurophysiol.* **85**(2), 926–937 (2001).

52. A. Korngreen and B. Sakmann, "Voltage-gated K^+ channels in layer 5 neocortical pyramidal neurones from young rats: subtypes and gradients," *J. Physiol. (Lond)* **525**, 621–639 (2000).

53. M. Migliore and G. M. Shepherd, "Emerging rules for the distributions of active dendritic conductances," *Nat. Rev. Neurosci.* **3**(5), 362–370 (2002).

54. M. Almog and A. Korngreen, "A quantitative description of dendritic conductances and its application to dendritic excitation in layer 5 pyramidal neurons," *J. Neurosci.* **34**(1), 182–196 (2014).

55. S. R. Williams and G. J. Stuart, "Backpropagation of physiological spike trains in neocortical pyramidal neurons: implications for temporal coding in dendrites," *J. Neurosci.* **20**(22), 8238–8246 (2000).

56. M. Migliore, "Modeling the attenuation and failure of action potentials in the dendrites of hippocampal neurons," *Biophys. J.* **71**(5), 2394–2403 (1996).

57. F. Ramon, R. W. Joyner, and J. W. Moore, "Propagation of action potentials in inhomogeneous axon regions," *Fed. Proc.* **34**(5), 1357–1363 (1975).

58. Y. Grossman, I. Parnas, and M. E. Spira, "Differential conduction block in branches of a bifurcating axon," *J. Physiol. (Lond)* **295**, 283–305 (1979).

59. A. Losonczy, J. K. Makara, and J. C. Magee, "Compartmentalized dendritic plasticity and input feature storage in neurons," *Nature* **452**(7186), 436–441 (2008).

60. F. W. Johenning et al., "Dendritic compartment and neuronal output mode determine pathway-specific long-term potentiation in the piriform cortex," *J. Neurosci.* **29**(43), 13649–13661 (2009).

61. B. J. Hoffman et al., "Localization and dynamic regulation of biogenic amine transporters in the mammalian central nervous system," *Front. Neuroendocrinol.* **19**(3), 187–231 (1998).

62. S. S. Wang and S. Thompson, "A-type potassium channel clusters revealed using a new statistical analysis of loose patch data," *Biophys. J.* **63**(4), 1018–1025 (1992).

63. I. L. Kopysova and D. Debanne, "Critical role of axonal A-type K^+ channels and axonal geometry in the gating of action potential propagation along CA3 pyramidal cell axons: a simulation study," *J. Neurosci.* **18**(18), 7436–7451 (1998).

64. M. Kollo, N. B. Holderith, and Z. Nusser, "Novel subcellular distribution pattern of A-type K+ channels on neuronal surface," *J. Neurosci.* **26**(10), 2684–2691 (2006).

65. K. Kerti, A. Lorincz, and Z. Nusser, "Unique somato-dendritic distribution pattern of Kv4.2 channels on hippocampal CA1 pyramidal cells," *Eur. J. Neurosci.* **35**(1), 66–75 (2012).

66. E. Guigon and Y. Burnod, "Modelling the acquisition of goal-directed behaviors by populations of neurons," *Int. J. Psychophysiol.* **19**(2), 103–113 (1995).

67. G. Winterer et al., "Cortical activation, signal-to-noise ratio and stochastic resonance during information processing in man," *Clin. Neurophysiol.* **110**(7), 1193–1203 (1999).

68. M. Rudolph and A. Destexhe, "Do neocortical pyramidal neurons display stochastic resonance?," *J. Comput. Neurosci.* **11**(1), 19–42 (2001).

69. H. Korn and P. Faure, "Is there chaos in the brain? II. Experimental evidence and related models," *C. R. Biol.* **326**(9), 787–840 (2003).

70. P. Yan et al., "Palette of fluorinated voltage-sensitive hemicyanine dyes," *Proc. Natl. Acad. Sci. U. S. A.* **109**(50), 20443–20448 (2012).

71. http://www.neuron.yale.edu.

72. http://senselab.med.yale.edu/senselab/modeldb/.

73. M. Migliore et al., "Role of an A-type K^+ conductance in the back-propagation of action potentials in the dendrites of hippocampal pyramidal neurons," *J. Comput. Neurosci.* **7**(1), 5–15 (1999).

Wen-Liang Zhou obtained his PhD degree from the University of Connecticut and now works in the laboratory of Marina Picciotto at Yale University.

Shaina M. Short obtained her PhD degree from the University of Connecticut and now works in the laboratories of Justus Verhagen and Gordon Shepherd at Yale University.

Matthew T. Rich obtained his master's degree from Hartford University and he is now a graduate student in the laboratory of Mary M. Torregrossa at the University of Pittsburgh.

Katerina D. Oikonomou obtained her PhD degree from the University of Connecticut and now works in the laboratories of Larry Hoffman and Felix Schweizer at UCLA.

Mandakini B. Singh is a PhD student in the neuroscience program at the University of Connecticut.

Enas V. Sterjanaj obtained his master's degree from Hartford University, currently works in the genetic testing lab at Charles River, and is applying for admission into a graduate PhD program.

Srdjan D. Antic is a researcher at the University of Connecticut, School of Medicine. He obtained an MD degree in medicine and an MS degree in biophysics at Belgrade University, Serbia. He was trained in several laboratories, including the laboratories of Dejan Zecevic (Yale University), Lawrence B. Cohen (MBL, Woods Hole), and Patricia Goldman-Rakic (Yale University).